

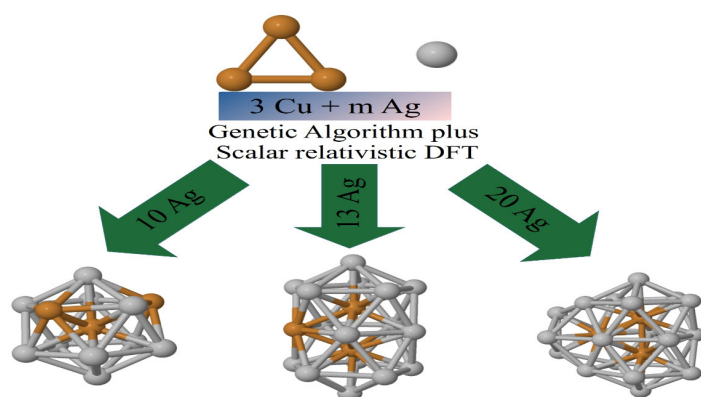
Full Paper | <http://dx.doi.org/10.17807/orbital.v13i3.1536>

A Detailed Theoretical Study of Cu_3Ag_m Bimetallic Clusters

Francinaldo dos Santos Leite ^a, Augusto César Azevedo Silva ^a, Caio Vinícius Caetano ^a, Adilson Luís Pereira Silva ^b, and Jaldyr de Jesus Gomes Varela Júnior* ^a

In this work, we explored the energy landscape and the effect of increasing the amount of Ag atoms over the segregation of Cu atoms in bimetallic clusters with compositions Cu_3Ag_m ($3 \geq m \geq 21$), using a genetic algorithm coupled with the Gupta potential to determine the most stable clusters. According to our results, the Ag atoms determine the magic compositions, which are the $\text{Cu}_3\text{Ag}_{10}$, $\text{Cu}_3\text{Ag}_{16}$ and $\text{Cu}_3\text{Ag}_{20}$ clusters. In all studied structures, the Cu atom establishes an interface with the Ag atoms or tends to form a core-shell structure with at least one Cu atom on the cluster surface. Scalar relativistic DFT calculations of the magic compositions reveal that these clusters have an electronic behavior similar to their pure Ag analogues.

Graphical abstract



Keywords

Copper
DFT
Genetic algorithm
Silver
Metallic cluster

Article history

Received 20 August 2020
Revised 10 February 2021
Accepted 22 March 2021
Available online 27 June 2021

Handling Editor: Paulo de Sousa Filho

1. Introduction

Clusters are atomic or molecular agglomerated constituted by few or many identical or different atoms [1, 2]. The possibility of modulating the properties of bimetallic clusters, specifically the coinage metals, has made the study of nanoclusters of these metals highly attractive from a theoretical and experimental viewpoint. In relation to copper-silver clusters, its potential applications has been much discussed, mainly in electrochemistry as a surface for CO oxidation [3-5] and a heterogeneous catalyst for water-gas shift reaction [6].

The computational treatment that the literature reports for

these clusters is only the calculation at DFT level (Density Functional Theory). In this methodology, through multiple attempts, the structures are modeled and the information about the local minimum of energy for each cluster is obtained. Heard and Johnston [7], through this methodology, have predicted the structure for the $\text{Cu}_m\text{Ag}_{(8-m)}$ clusters, which is valid for small clusters [8-11]. However, according to the amount of the atoms increases, the prediction of the geometries becomes a more complex task, since the number of topological structural isomers (homotopes) increases [12], therefore it is necessary to use search algorithms such as the evolutionary genetic algorithms (GA).

^a Programa de Pós-Graduação em Química, Universidade Federal do Maranhão, São Luís – MA, Brazil. ^b Departamento de Química, Universidade Estadual do Maranhão, São Luís – MA, Brazil. *Corresponding author. E-mail: jaldyr.varela@ufma.br

In this context, the search of the cluster geometries, using evolutionary genetic algorithms (GA) as a primary stage for a later stage of application at a higher level of theory, results in a computational time gain, because the quantum methodologies will be used to calculate the corresponding structure to the putative global minimum and not for structures that correspond to local minimums [13]. Thus, the studies that use genetic algorithms to scan structures, or methods such as molecular dynamics [14] are well received by the literature, and are widely used to describe structures of larger clusters [15-17].

In relation to geometry the literature widely shows that small Cu-Ag clusters have planar geometry [18], but with a tendency to form three-dimensional structures as suggested by some DFT-based studies [7, 16, 19, 20]. However, in studies based on genetic algorithms (GA) coupled with the Gupta potential, this tendency is reversed, in which the three-dimensional structures for small clusters are revealed as global minimums and as the amount of atoms increases, the determined structures tend to become more complex [1, 17, 21, 22]. Mingos [23] proposed that in bimetallic silver clusters as from 19 atoms, the characteristic patterns would be fusions of simpler structures. Nevertheless, could bimetallic

Cu-Ag clusters also have this tendency? In order to answer this question, this study aimed to determine the geometry corresponding to the global minimums of bimetallic clusters with Cu_3Ag_m ($3 \leq m \leq 21$) composition, using the combined GA-DFT strategy, which was used to optimize the magic compositions.

2. Results and Discussion

2.1 Analysis of the energetic stability of Cu_3Ag_m clusters

Firstly, for each bimetallic cluster composition, the genetic algorithm (GA) was used to generate all possible geometries. And the best geometry for each composition was chosen as the structure that was found most in each cycle, as described in the methodology section 3.1, item 4. Thus, at the end of 30 cycles for each composition, some geometries were found more than 90% of times as the most stable for most compositions. Therefore, we can infer that these are the best geometries that correspond to the most stable structures for each bimetallic cluster composition, which are illustrated in Figure 1. For this reason, these structures were chosen to be studied throughout this work.

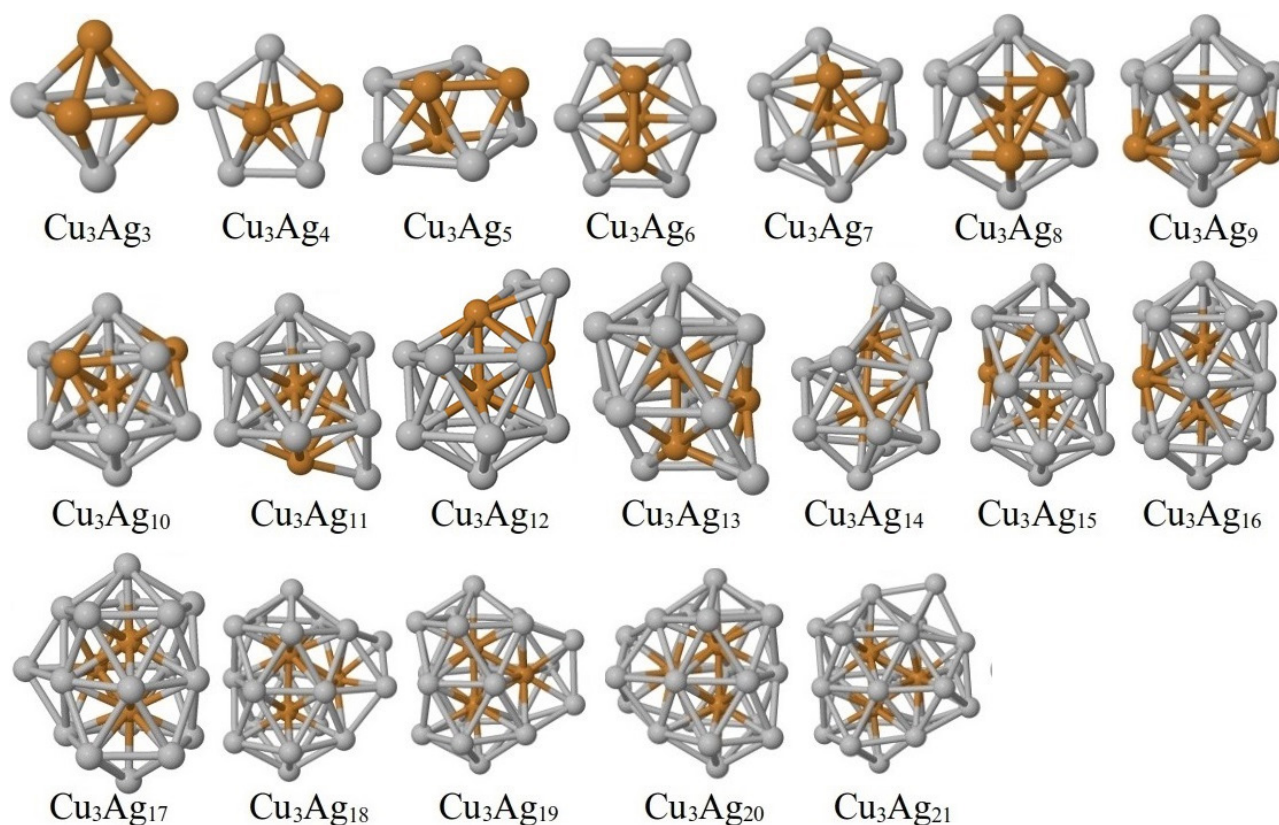


Fig. 1. Optimized structures of the Cu_3Ag_m clusters (with $3 \leq m \leq 21$). The grey and brown balls represent the Ag and Cu atoms, respectively.

To find the magic compositions, we plotted the second energy difference (Δ_2E) of the Cu_3Ag_m bimetallic clusters, as shown in Figure 2, where all compositions above the red dotted line are more stable structures in relation to their nearest neighbors. The maximum points represent the magic compositions, which are the $\text{Cu}_3\text{Ag}_{10}$, $\text{Cu}_3\text{Ag}_{16}$ and $\text{Cu}_3\text{Ag}_{20}$ clusters. We also noticed that these same compositions also correspond to the most stable monometallic clusters of Ag (Ag_{13} , Ag_{19} and Ag_{23}), so this suggests that for the studied Cu_3Ag_m clusters, the Ag atom determines the magic

compositions, i.e., the clusters with the most particular stabilities. On the other hand, monometallic clusters of Ag as well as their nanoparticles are highly stable structures [24], therefore, Ag atoms are also expected to determine the stability of bimetallic clusters.

In Figure 1, we also can see that the bimetallic clusters with Cu_3Ag_m composition have a tendency to segregate. This effect can be explained by the mixing energy of the clusters [19, 20], as shown in Figure 3 (a), which remained negative according to the amount of Ag added to the system. This

suggests that the structures with Ag excess tend to facilitate the segregation of Ag by Cu, that is, a clear tendency to encompass planar Cu atoms, as shown in theoretical work of Núñez and Johnston [16]. The segregation tendency can also be understood as a function of the binding energy of the cluster [see Figure 3 (b) and Figure 4], the higher the tendency to segregate, that is, in clusters with high binding energy, the segregation tendency is high for the silver atom to move to the surface [1, 16, 19]. On the other hand, the binding energies of the copper monometallic clusters are greater than the silver monometallic clusters, as shown in Figure 4, which suggests that these bonds are formed first and maintained after the formation of Cu-Ag bonds.

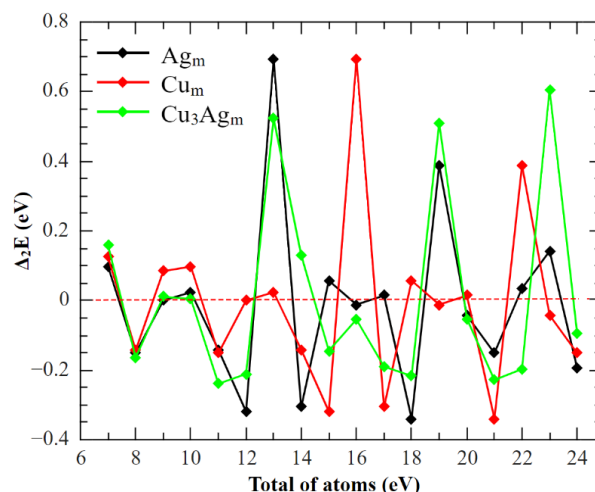


Fig. 2. Second energy difference plot (Δ_2E) for Cu_3Ag_m bimetallic clusters and their pure Cu and Ag analogues, using the energies obtained for each structure at the GA level.

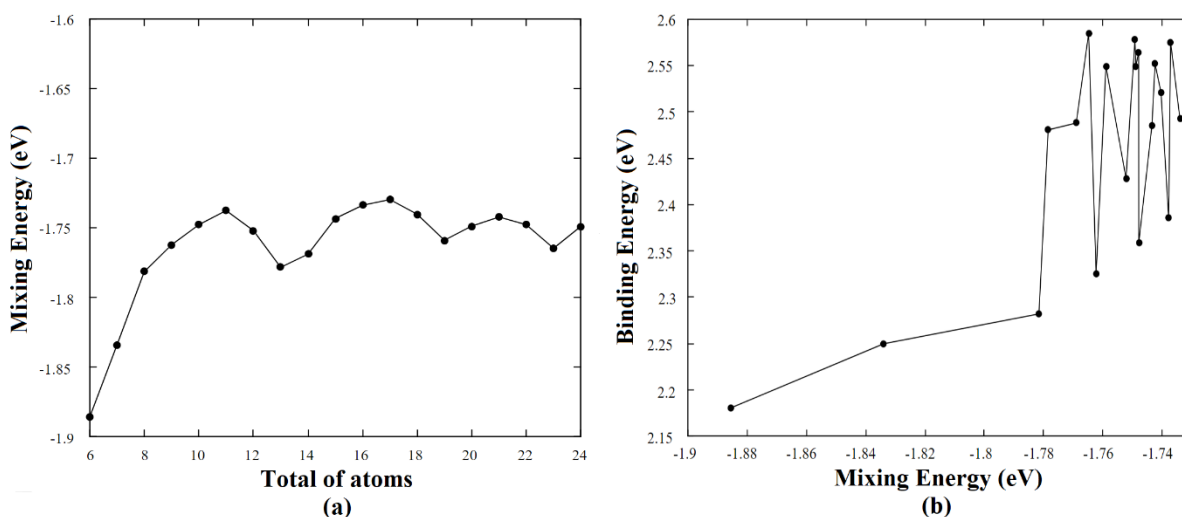


Fig. 3. (a) Mixing energy of the Cu_3Ag_m clusters and (b) correlation between the mixing energy and the binding energy per atom of the Cu_3Ag_m bimetallic clusters.

Silver has the natural tendency to arrange itself as a layer in bimetallic clusters of Cu and Ag [15, 25], and in the absence of enough Ag excess for this, segregated subcluster structures appear, as in the structure Cu_3Ag_3 , where the Cu and Ag atoms are in equal quantity. In structures with a high amount of Ag atoms, they become segregated clusters. In structures close to those with the highest stability and, therefore, with geometries close to an icosahedron, we find a strengthening of the Ag-Ag bond. Thus, the closed planar structure of Cu_3 is ruptured and segregation structures typical of a core-shell can be found, particularly in the Cu_3Ag_{10} cluster, where the Cu atoms begin to localize more and more internally in the cluster.

The binding energies per atom for the bimetallic clusters, calculated using equation (5), are between the Cu_m and Ag_m binding energies (see Figure 4). This is one of the prerequisites to occur segregation in a bimetallic cluster [1], therefore, in these clusters there is not a competition between the homonuclear and heteronuclear bonds, which widely favors the segregated structures. In addition, Ag has a lower average surface energy than Cu [15, 16], which also contributes to the segregation of the studied structures. And in the considered range, from 6 to 21 atoms, there are no structures with a tendency to form mixtures, i.e., structures

where the Cu and Ag atoms arrange themselves randomly in the cluster.

The segregation also determines the geometry of the bimetallic clusters, therefore, the Cu_3Ag_3 and Cu_3Ag_4 have regular octahedral geometries, although the Cu_3Ag_4 has an octahedral geometry a little bit flattened as shown in Figure 1. The Cu_3Ag_5 , Cu_3Ag_6 , Cu_3Ag_7 and Cu_3Ag_8 clusters have irregular octahedral geometries (see Figure 1). The Cu_3Ag_{11} cluster has a cuboctahedral structure, which is very similar to the Cu_3Ag_{10} structure, but the latter has a geometry closer to an icosahedral than to a cuboctahedral. For this reason, this cluster is one of the most stable, since in icosahedral structures the structure-related steric effects are small, which is one of the factors that partly justify the high stability of this structure when compared to other studied clusters. In larger structures, the preferred geometry is the interpenetrated icosahedron, which consists of the fusion of two icosahedrons, or even interpenetrated cuboctahedrons. These results confirm some studies predicted in the literature, in which clusters with a large amount of atoms present a high tendency to have geometries resulting from the fusion of stable structures, such as icosahedrons or interpenetrated cuboctahedrons [22, 23, 26, 27].

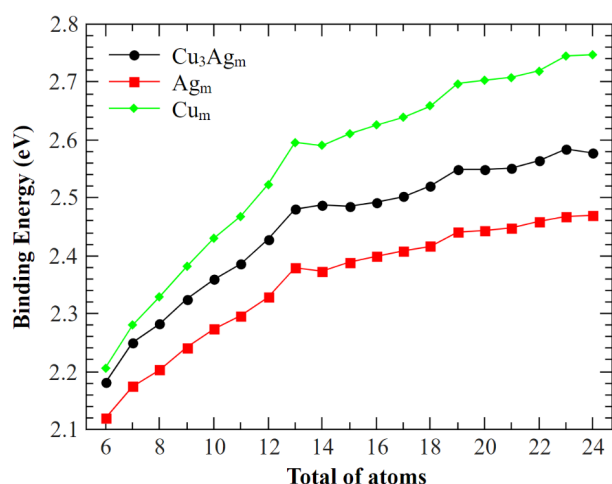


Fig. 4. Binding energy per atom of the Cu_3Ag_m bimetallic clusters.

Table 1. Average length of the Ag-Ag, Cu-Cu and Ag-Cu bonds of the studied bimetallic clusters obtained at the GA and DFT levels. The values in parentheses correspond to those obtained at the DFT level.

Cluster	Ag-Ag ^a (Å)	Deviation (%)	Cu-Cu ^b (Å)	Deviation (%)	Cu-Ag ^c (Å)	Deviation (%)
$\text{Cu}_3\text{Ag}_{10}$	2.80 (2.89)	-3.09 (0.30)	2.53 (*)	-0.98 (*)	2.63 (2.73)	-3.45 (-0.24)
$\text{Cu}_3\text{Ag}_{16}$	2.83 (2.90)	-2.08 (-0.28)	2.52 (2.55)	-1.29 (-0.30)	2.64 (2.76)	-3.19 (-1.27)
$\text{Cu}_3\text{Ag}_{20}$	2.83 (2.91)	-2.01 (-0.58)	2.51 (2.56)	-1.75 (-0.11)	2.63 (2.71)	-3.38 (0.64)

* This value for the Cu-Cu bond was not found at DFT level in this cluster. ^a The reference value for the Ag-Ag bond length is 2.89 Å [28]. ^b The reference value for the Cu-Cu bond length is 2.56 Å [28]. ^c The reference value for the Cu-Ag bond length is 2.72 Å [28].

Some relevant electronic properties of the magic composition bimetallic clusters are shown in Table 2, where we can see that the $\text{Cu}_3\text{Ag}_{10}$ cluster presents a high vertical ionization potential and an intermediate electronic affinity between the $\text{Cu}_3\text{Ag}_{16}$ and $\text{Cu}_3\text{Ag}_{20}$ clusters, which implies that this cluster would not be appropriate for adsorption, because its high ionization potential could prevent the chemisorption of specific molecules in the cluster.

Table 2. Electronic properties of the $\text{Cu}_3\text{Ag}_{10}$, $\text{Cu}_3\text{Ag}_{16}$ and $\text{Cu}_3\text{Ag}_{20}$ clusters.

Cluster	Vertical Ionization potential (eV)	Vertical Electronic Affinity (eV)	Gap (eV)	Magnetic Moment (μ_B)
$\text{Cu}_3\text{Ag}_{10}$	5.59	-1.93	2.03	0.00
$\text{Cu}_3\text{Ag}_{16}$	5.29	-1.95	0.32	0.00
$\text{Cu}_3\text{Ag}_{20}$	4.88	-1.72	0.14	0.00

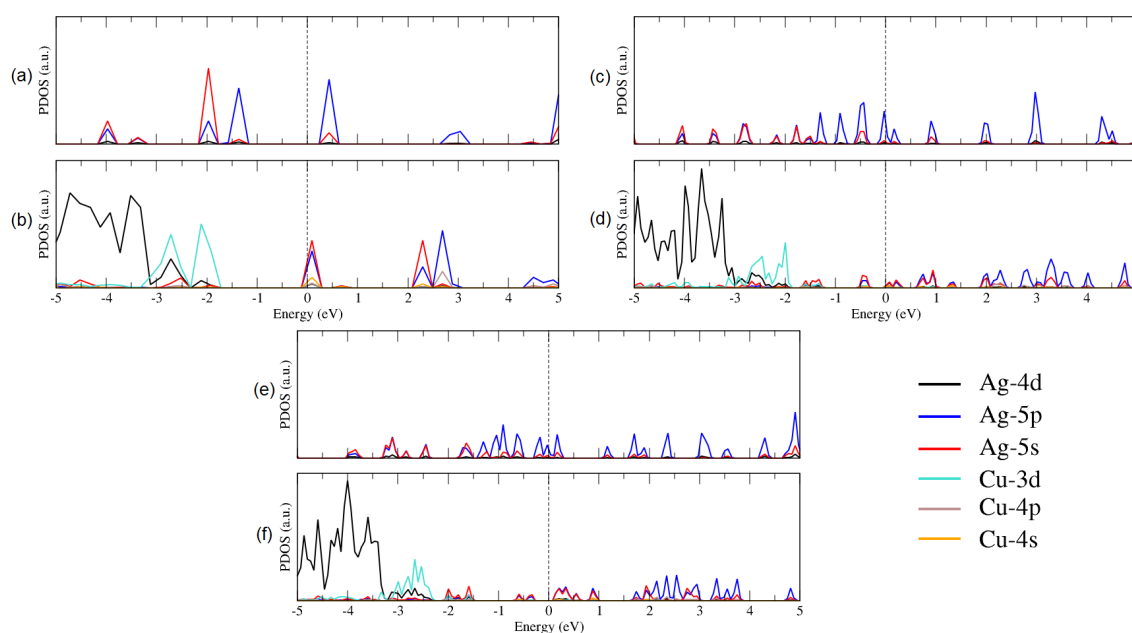


Fig. 5. Projected density of states (PDOS) for the s, p and d orbitals of Ag and Cu atoms in the (a) Ag_{13} , (b) $\text{Cu}_3\text{Ag}_{10}$, (c) Ag_{19} , (d) $\text{Cu}_3\text{Ag}_{16}$, (e) Ag_{23} and (f) $\text{Cu}_3\text{Ag}_{20}$ structures. The vertical dotted line corresponds to the Fermi level.

The PDOS analysis of the magic composition bimetallic clusters (see Figure 5) shows that the d orbitals of both metal atoms contribute to more internal energy levels as the amount of Ag increases. The highest occupied orbital (HOMO) of $\text{Cu}_3\text{Ag}_{10}$ has a high contribution from the d orbitals of the Cu with low contributions of the d orbitals of the Ag, while in the $\text{Cu}_3\text{Ag}_{16}$ and $\text{Cu}_3\text{Ag}_{20}$ clusters, the HOMO has contribution exclusively from the s and p orbitals of the Ag atoms. It is important to note that the p orbitals of these metals contributed to the formation of many energy levels, which is not expected because these orbitals are empty in the valence shell of each metal.

The Ag_{13} is a semiconductor [see Figure 5 (a)] while the Ag_{19} and Ag_{23} are metallic systems, because the Fermi level is crossing an energy level, as shown in Figures 6(c) and 6(d). The band gap of the bimetallic cluster decreases as the amount of Ag atoms increases, as we can see in the Table 2 and with the PDOS analysis of these systems, thus we can infer that there is a tendency of the Cu_3Ag_m clusters become metallic systems as their pure Ag analogues. This is already expected because in these structures the degree of copper

exposure to the surface is very low. Therefore, as the amount of Ag atoms increases, these clusters would behave as their corresponding pure Ag analogues.

This tendency is more evident when we study the infrared spectra of these clusters in relation to their pure Ag analogues (Ag_{13} , Ag_{16} and Ag_{23}) and the Cu_3 cluster, as shown in Figure 6. We verified that the addition of Ag to the Cu_3 cluster causes it to lose its Cu_3 properties. However, the strongest Cu_3 band around 150 cm^{-1} always remains in the vibrational spectrum, because in these clusters, the closed and planar Cu_3 primary structure was maintained, except in the $\text{Cu}_3\text{Ag}_{10}$ cluster, in which the Cu_3 planar structure was broken, and therefore its vibrational spectrum is practically similar to its pure Ag analogue, in which the maximums correspond to displacements of Ag-Ag bonds. The last peaks found in the region between 175 to 250 cm^{-1} correspond to the Ag-Cu bonds, however, these maximums are similar in the $\text{Cu}_3\text{Ag}_{10}$ and $\text{Cu}_3\text{Ag}_{16}$ clusters, but are more widely spaced in the $\text{Cu}_3\text{Ag}_{20}$, because in this cluster the amount of Cu-Ag bonds is lower than in the others two clusters, which causes the bands to occur between 300 to 400 cm^{-1} .

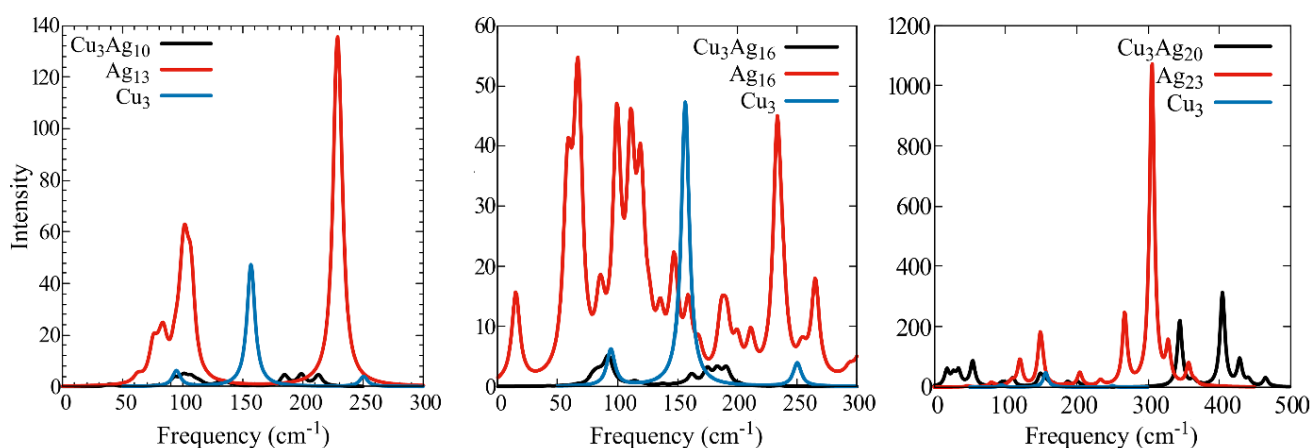


Fig. 6. Infrared spectra of the most stable bimetallic clusters and its pure Ag analogues in comparison with the Cu_3 cluster.

3. Material and Methods

3.1 Genetic Algorithm

The structures of the Cu_3Ag_m bimetallic clusters were generated through a planar structure with a fixed composition of Cu_3 , in which were added between 3 to 21 Ag atoms to form initially a core-shell structure through a genetic algorithm (GA) proposed by Pereira and Marques [29-32]. This algorithm had been modified to allow the calculation of Cu_3Ag_m clusters structures. In general, we can say that GA determines the structures with the lowest potential energy for a given configuration, through the following steps:

1. An initial population of 100 individuals is generated, corresponding to candidates for the global minimum. Each individual consists of a fixed amount of atoms, which corresponds to the total number of Cu and Ag atoms in the structure. The positions of the Cu atoms are fixed, allowing little variation, while the positions of the Ag atoms are variable.
2. When the initial population is generated, a minimization using the L-BFGS optimization algorithm is performed. The fitness of each result is obtained through a specific potential, which in

this case corresponds to the Gupta potential [33].

3. There is a stage of generation of descendants, in which they compete with each other. This stage is subdivided into 4 substeps: (i) Selection tournament: five clusters are formed and two of them are chosen. (ii) The crossover and mutation operators are applied to the clusters. The crossover operator generates a cluster with less potential energy, while the mutation operator changes the positions between the Cu and Ag atoms in the structure generated by the crossover. (iv) A post optimization operator is applied to each descendant, and only the best solution is maintained.
4. Item 3 is repeated in a self-consistent way for 30 times, and in each cycle the function that describes the potential is evaluated 10^8 times, with a convergence criterion of 10^{-5} eV between each global putative minimum.

3.2 Potential Model

The metallic bonds were described by the Gupta potential [33], which consists of a consequence of the second-moment approximation to a tight-binding Hamiltonian, as described by the following equations:

$$V_{cluster} = \sum_{i=1}^N (V_i^{band} - V_i^{repulsion}) \text{ eq. (1)}$$

where, the terms for band potential, as well as for the repulsion potential are given below:

$$V_i^{band} = - \sqrt{\sum_{j \neq i} \xi_{\alpha,\beta}^2 \exp \left[-2q_{\alpha,\beta} \left(\frac{r_{ij}}{r_{\alpha,\beta}^0} - 1 \right) \right]} \text{ eq. (2)}$$

$$V_i^{repulsion} = \sum_{j \neq i} A_{\alpha,\beta} \exp \left[-p_{\alpha,\beta} \left(\frac{r_{ij}}{r_{\alpha,\beta}^0} - 1 \right) \right] \text{ eq. (3)}$$

In the equations (2) e (3), the A, p, ξ q, r_0 are independent parameters of the potential and specific to each interaction. In this work, the parameters used for the studied interactions (Cu-Cu, Cu-Ag and Ag-Ag) are shown in Table 3.

Table 3. Gupta potential parameters used in this work [34].

Parameters	Cu-Cu	Cu-Ag	Ag-Ag
A (eV)	2.278	2.805	3.180
p	10.960	10.700	10.850
q	1.2240	1.2274	1.1895
ξ	0.0855	0.0980	0.1031
R_0 (Å)	2.55600	2.72405	2.89210

3.3 Energetic analysis and electronic properties

The structures corresponding to the magic compositions (obtained at the GA level) were refined at the DFT level through the SIESTA 3.2 software [35], using the PBE functional for the exchange-correlation term and a double-zeta basis set with polarization function (DZP) for the Cu and Ag atoms. In addition, relativistic pseudopotentials were also used, therefore, the relativistic scalar effects pertinent to copper and silver atoms [15] were also considered.

The energetic analysis of the clusters was performed by the second energy difference (Δ_2E) at the GA level, which was used to identify the structures with greater stability, that is, the magic compositions, and is defined by equation (4):

$$\Delta_2E = E(Cu_3Ag_{m+1}) + E(Cu_3Ag_{m-1}) - 2E(Cu_3Ag_m) \text{ eq. (4)}$$

where, $E(Cu_3Ag_m)$, $E(Cu_3Ag_{m+1})$ and $E(Cu_3Ag_{m-1})$ correspond to the total potential energies of the Cu_3Ag_m , Cu_3Ag_{m+1} and Cu_3Ag_{m-1} cluster, respectively. The cluster segregation analysis, that is, its tendency to form heterogeneous phases, were determined by its mixing energy (E_{mix}) [36] and binding energy (E_b) [1], expressed by the equation (5) and (6):

$$E_{mix} = \frac{1}{N} \left\{ E(Cu_3Ag_m) - \frac{1}{N} [m \cdot E(Cu_N) + (N - m) \cdot E(Ag_N)] \right\} \text{ eq. (5)}$$

$$E_b = -\frac{V}{N} \text{ eq. (6)}$$

where, N represents the total number of atoms in the cluster while m represents the amount of Ag in that same cluster. Furthermore, the band gap was calculated using the projected

density of states (PDOS), the magnetic moment was obtained through the Mülliken population, and the infrared spectra were generated by the Gaussian 09 package using the same basis set (DZP) and exchange-correlation functional (PBE) used in the SIESTA calculations.

4. Conclusions

The bimetallic clusters of Cu_3Ag_m composition ($3 \leq m \leq 21$) tend to present the segregated subcluster pattern, where Ag atoms form an interface with Cu atoms. As the amount of Ag atoms increases, the clusters have a tendency to present similar structures to a core-shell with some copper atoms exposed, which can be noted in the oscillations obtained in the mixing energy analysis. The geometries of larger clusters tend to be the result of the fusion of simpler cluster structures. In particular, the Cu_3Ag_{10} cluster has an icosahedral structure, while the other magic compositions clusters (Cu_3Ag_{16} and Cu_3Ag_{20}) have structures that resemble a fusion of two icosahedrons, which partially explains why these structures are also stable, because icosahedral structures are naturally stable. In addition, these most stable clusters (Cu_3Ag_{10} , Cu_3Ag_{16} and Cu_3Ag_{20}) tend to behave as their pure Ag analogues, as verified in the PDOS and IR analyzes at the limit where there is a large excess of Ag in the cluster

Acknowledgments

The authors are grateful for the financial support provided by CNPq, CAPES and FAPEMA.

Author Contributions

Francinaldo dos Santos Leite: Investigation, Writing - original draft, Visualization. Augusto C. Azevedo Silva: Investigation, Writing - review & editing. Caio V. Caetano: Investigation and Software. Adilson L. P. Silva: Investigation and Software. Jaldyr de J. G. Varela Júnior: Conceptualization, Methodology, Resources, Supervision and Funding acquisition.

References and Notes

- Ferrando, R.; Jellinek, J.; Johnston, R. L. *Chem. Rev.* **2008**, *108*, 845. [\[Crossref\]](#)
- Johnston, R. L. *Dalton Trans.* **2003**, 4193. [\[Crossref\]](#)
- Zhang, Y.; He, X. *Chem. Phys. Lett.* **2017**, *686*, 116123. [\[Crossref\]](#)
- Mahara, Y.; Ishikawa, H.; Ohyama, J. Sawabe, K.; Satsuma, A. *Catal. Today.* **2015**, *265*, 2. [\[Crossref\]](#)
- Banda-Alemán, J. A.; Orozco G.; Bustos, E.; Sepúlveda, S.; Manríquez, J. J. *CO₂ Util.* **2018**, *27*, 459. [\[Crossref\]](#)
- Guo, L.; Li, A.; An, X.; Cao, Z.; Liu, N. *Int. J. Hydrog. Energy* **2015**, *40*, 8330. [\[Crossref\]](#)
- Heard, C. J.; Johnston, R. L. *Eur. Phys. J. D.* **2013**, *67*, 34. [\[Crossref\]](#)
- Zhou, Y. H.; Zeng, Z.; Ju, X. *Microelectronics J.* **2009**, *40*, 832. [\[Crossref\]](#)
- Ma, W.; Chen, F. *J. Alloys Compd.* **2012**, *541*, 79. [\[Crossref\]](#)
- Lou, X.; Gao, H.; Wang, W.; Xu, C.; Zhang, H.; Zhang, Z. *J. Mol. Struct. THEOCHEM.* **2010**, *959*, 75. [\[Crossref\]](#)

- [11] García-Rodríguez, D. E.; Mendoza-Huizar, L. H.; Díaz, C. *Appl. Surf. Sci.* **2017**, *412*, 146. [\[Crossref\]](#)
- [12] Momin, T.; Bhowmick, A. *J. Alloys Compd.* **2013**, *559*, 24. [\[Crossref\]](#)
- [13] Zhao, J.; Shi, R.; Sai, L.; Huang, X.; Su, Y. *Mol. Simul.* **2016**, *7022*, 111. [\[Crossref\]](#)
- [14] Li, S.; Qi, W.; Peng, H.; Wu, J. *Comput. Mater. Sci.* **2015**, *99*, 125. [\[Crossref\]](#)
- [15] Molayem, M.; Grigoryan, V.G.; Springborg, M. *J. Phys. Chem. C* **2011**, *115*, 22148. [\[Crossref\]](#)
- [16] Nunez, S.; Johnston, R. L. *J. Phys. Chem. C* **2010**, *114*, 13255. [\[Crossref\]](#)
- [17] Bochicchio, D.; Ferrando, R.; Panizon, E.; Rossi, G. *J. Phys. Condens. Matter* **2015**, *28*, 64005. [\[Crossref\]](#)
- [18] Kilimis, D. A.; Papageorgiou, D. G. *Eur. Phys. J. D* **2010**, *56*, 189. [\[Crossref\]](#)
- [19] Li, W.; Ding, L.; Wang, K.; Wang, W.; Zhang, S. *Mater. Today Commun.* **2020**, *25*, 101248. [\[Crossref\]](#)
- [20] Rao, Y.; Lei, Y.; Cui, X.; Liu, Z.; Chen, F. *J. Alloys Compd.* **2013**, *565*, 50. [\[Crossref\]](#)
- [21] Bochicchio, D.; Ferrando, R.; Panizon, E.; Rossi, G. *J. Phys. Condens. Matter* **2016**, *28*, 064005. [\[Crossref\]](#)
- [22] Rapallo, A.; Rossi, G.; Ferrando, R.; Fortunelli, A.; Curley, B. C.; Lloyd, L. D.; Tarbuck, G. M.; Johnston R. L. *J. Chem. Phys.* **2005**, *122*, 194308. [\[Crossref\]](#)
- [23] Mingos, D. M. P. *Dalton Trans.* **2015**, *44*, 6680. [\[Crossref\]](#)
- [24] Desireddy, A.; Conn, B. E.; Guo, J.; Yoon, B.; Barnett, R. N.; Monahan, B. M.; Kirschbaum, K.; Griffith, W. P.; Whetten, R. L.; Landman, U.; Bigioni, T. P. *Nature* **2013**, *501*, 399. [\[Crossref\]](#)
- [25] Moreno, V.; Creuze, J.; Berthier, F.; Mottet, C.; Trégliat, G.; Legrand, B. *Surf. Sci.* **2006**, *600*, 5011. [\[Crossref\]](#)
- [26] Ferrando, R.; Fortunelli, A.; Johnston, R. L. *Phys. Chem. Chem. Phys.* **2008**, *10*, 640. [\[Crossref\]](#)
- [27] Panizon, E.; Ferrando, R. *Nanoscale* **2016**, *8*, 15911. [\[Crossref\]](#)
- [28] Duan, D.; Liu, H.; You, X.; Wei, H.; Liu, S. *J. Power Sources* **2015**, *293*, 292. [\[Crossref\]](#)
- [29] Marques, J. M. C.; Pereira, F. B. *Chem. Phys. Lett.* **2010**, *485*, 211. [\[Crossref\]](#)
- [30] Marques, J. M. C.; Pereira, F. B. *J. Comput. Chem.* **2013**, *34*, 505. [\[Crossref\]](#)
- [31] Marques, J. M. C.; Pereira, F. B. *J. Mol. Liq.* **2015**, *210*, 51. [\[Crossref\]](#)
- [32] Zanvettor, C. M. A.; Marques, J. M. C. *Chem. Phys. Lett.* **2014**, *608*, 373. [\[Crossref\]](#)
- [33] Gupta, R. P. *Phys. Rev. B* **1981**, *23*, 6265. [\[Crossref\]](#)
- [34] Cleri, F.; Rosato, V. *Comput. Simul. Mater. Sci.* **1991**, *205*, 233. [\[Crossref\]](#)
- [35] Soler, J. M.; Artacho, E.; Gale, J. D.; García, A.; Junquera, J.; Ordejón, P.; Sánchez-Portal, D. *J. Physics Condens. Matter* **2002**, *14*, 27. [\[Crossref\]](#)
- [36] Sahoo, S.; Rollmann, G.; Entel, P. *Phase Transitions* **2006**, *79*, 693. [\[Crossref\]](#)

How to cite this article

Leite, F. S.; Silva, A. C. A.; Caetano, C. V.; Silva, A. L. P.; Varela Júnior, J. J. G. *Orbital: Electron. J. Chem.* **2021**, *13*, 212. DOI: <http://dx.doi.org/10.17807/orbital.v13i3.1536>